Earth Planet. Sci. Lett. 652 (2025) 119195

Contents lists available at ScienceDirect

Earth and Planetary Science Letters

journal homepage: www.elsevier.com/locate/epsl

Evidence for the role of tropical plumes in driving mid-Holocene north-west Sahara rainfall

Hamish O. Couper [a], Christopher C. Day [a,*], Julia J. Barrott [a,b], Samuel J. Hollowood [a], Stacy A. Carolin [d], Ben Lovett [e], Abdeljalil Bouzouggar [c], Nick Barton [d], Gideon M. Henderson [a]

[a] Department of Earth Sciences, University of Oxford, Oxford, OX1 3AN, UK
[b] Research Fellow, Stockholm Environment Institute, Oxford, OX2 7JT, UK
[c] Institut National des Sciences de l'Archéologie et du Patrimoine, Rabat-Instituts, Rabat, Morocco
[d] School of Archaeology, University of Oxford, Oxford, OX1 3TG, UK
[e] Northern Caverneers Caving Club, Legana, 7277, Tasmania, Australia

A R T I C L E I N F O

Edited by Dr Y Asmerom

Keywords:
Speleothem
Sahara
Holocene
Paleoclimate
African humid period
Paleohydrology

A B S T R A C T

The West African Monsoon (WAM), Atlantic north-westerlies and Mediterranean cyclones are significant sources of rainfall in north-west Africa, supplying moisture to the fringes of the Sahara. Rainfall patterns and the extent of the desert vary through time with strong evidence of a wetter Sahara during the early- to mid-Holocene (widely referred to as the African Humid Period). North of 28°N there is a particular lack of palaeorainfall reconstructions, with higher spatial- and temporal-resolution required to constrain the mechanisms responsible for past sub-tropical climate change, and the impacts of environmental change on human developments. We provide palaeorainfall reconstructions from stalagmites from today's arid north-west Sahara, inland from the coast and south of the Atlas Mountains in Morocco (30–32°N). The records show increased rainfall between 8.7–4.3 kyr BP. The timing, and oxygen isotopes of the speleothem growth, in comparison with other records, strongly suggest that South-of-Atlas rainfall continued after the decline of the West African Monsoon in the mid-Holocene. We propose that additional rainfall was supplied by increased tropical-plume rainfall in the South-of-Atlas region. We suggest that an increased North-South inter-hemispheric temperature anomaly, shifting the ITCZ northwards, increased the supply of tropical-moisture to tropical-plumes. For the first time this study provides evidence supporting tropical-plumes as an additional source of past-rainfall, helping to reconcile palaeo-archives and modelling studies. Increased South-of-Atlas rainfall improved habitability and increased recharge to rivers flowing south into the Sahara, which likely facilitated connectivity through the Sahara, during a key period in the development of land use and animal production.

1. Introduction

There is strong proxy evidence that regions in today's Sahara experienced wetter conditions in the early to mid-Holocene (e.g. Gasse, 2000; Cremaschi et al., 2010; Adkins et al., 2006), with wide-ranging hypotheses regarding the underlying mechanisms. The main difference between studies are variations in the proposed source and extent of the expansion of rainfall, with suggestions of the West African Monsoon expanding northwards (e.g. Tierney et al., 2017), of winter Mediterranean cyclones extending southwards, and even of overlap between both systems (Cheddadi et al., 2021). There is also a lack of consensus on the nature and extent of past vegetation, with some studies suggesting that vegetation replaced desert-biome at all latitudes (e.g. Jolly et al., 1998), and others finding that the desert-biome persisted within varying latitudes even during the early to mid-Holocene wetter conditions (Kutzbach et al., 2020; Dallmeyer et al., 2020).

The most widely discussed source of increased past rainfall is the intensification and northwards expansion of the West African Monsoon (WAM), although studies disagree on details such as the northern limit of monsoonal rain, i.e. whether this extended beyond 30°N (Tierney et al., 2017; Sha et al., 2019; Pausata et al., 2017), or remained between 15°N and 25°N (Dallmeyer et al., 2020; Braconnot et al., 2007; Perez-Sanz et al., 2014; Quade et al., 2018; Boateng et al., 2024). The source of mid-Holocene moisture at subtropical latitudes (>30°N) is

* Corresponding author.
E-mail address: chris.day@earth.ox.ac.uk (C.C. Day).

https://doi.org/10.1016/j.epsl.2024.119195
Received 7 June 2024; Received in revised form 19 December 2024; Accepted 27 December 2024
Available online 9 January 2025

particularly uncertain. Whilst there are reports of increased rainfall at these higher latitudes (Tierney et al., 2017; Sha et al., 2019; Ait Brahim et al., 2023), there are differences in the interpreted mechanism and source of rainfall. There are also differences between model-studies regarding the amount and northwards-extent of increased WAM rainfall (e.g. Pausata et al., 2016; Hopcroft and Valdes, 2019), with uncertainty introduced by complex feedbacks between environmental properties e.g. dust-characteristics, dust-cloud interactions, sea surface temperature (Pausata et al., 2020). The strength and latitudinal extent of the annual WAM is complex, influenced by multiple external and internal controls including boreal summer insolation, the intensity and position of the Tropical Easterly Jet (TEJ), the Saharan Heat Low, and the position of the Intertropical Convergence Zone (ITCZ) (Raj et al., 2019). Recent studies highlight this complexity and the lack of a simple relationship between ITCZ and WAM (Geen et al., 2020).

In addition to the WAM, a smaller number of studies propose northern sources of rainfall, e.g. Mediterranean Cyclones or Atlantic North Westerlies (ANW), expanding southwards, supplying greater rainfall to the northern Sahara (Gasse, 2000; Cheddadi et al., 2021; Ait Brahim et al., 2023; Kutzbach et al., 1996). Some even suggest periods of overlap of northern and southern sources of rainfall within a given year (Cheddadi et al., 2021), leading to dual-season rainfall, in support of proposals that vegetation was more abundant at all latitudes.

A less widely discussed source of rainfall, is increased subtropical rainfall from moisture sourced in the tropics. This source presently supplies a small amount of rainfall to subtropical latitudes such as the South-of-Atlas region (Thepenir and Cruette, 1981; Knippertz, 2007; Iskenderian, 1995). This type of rainfall is known under many different names including tropical depressions (Maley, 1977), moisture bursts (Mcguirk et al., 1987), Saharan disturbances (Dubief and Queney, 1935), and Tropical-Extratropical Interactions (Knippertz, 2007). From hereon we use Tropical Plumes 'TP' to refer to this mechanism of exporting tropical moisture to the sub-tropics. The mechanism underlying TP-rainfall involves equatorward, upper-level troughs penetrating the tropics, picking up convected moisture from the tropics before transporting moisture back to the sub-tropics (e.g. Mcguirk et al., 1987; Knippertz, 2003). The band of upper-level clouds can be 2,000–16,000 km long, hundreds of km wide, with a SW-NE orientation in the NH, with event durations typically 3–9 days (Mcguirk et al., 1987; Ziv, 2001). In NW Africa, the highest relative importance of TP rainfall is in the southern foothills of the Atlas, where orographic effects and upper-level divergence enable precipitation to form from the moisture transported northward by the TP mechanism (Maley, 1977; Knippertz, 2003).

Some of the pioneering evidence of enhanced rainfall in the Sahara is from the measured fluxes of terrestrial-sourced dust from marine core archives (e.g. deMenocal et al., 2000; Adkins et al. 2006; McGee et al. 2013). However, these marine-based records do not determine precisely where increased-rainfall occurred. Speleothems, secondary calcium carbonate that forms in caves, including stalagmites, are alternative climate archives that have not previously been used in the drier, inland regions of the north-west Sahara. Stalagmites, in arid locations are uniquely capable of directly recording periods when local rainfall rises above a threshold level (Vaks et al., 2010). The stalagmite-$CaCO_3$ that forms during these wetter, non-arid periods, can be precisely dated with U-Th radiometric dating. Stable isotope measurements provide additional environmental information, with oxygen isotopes helping to identify the isotopic signature of rainfall sources. Stalagmites are therefore ideally suited for higher-resolution investigations of North African rainfall changes.

Here we produce stalagmite-based reconstructions of palaeo-rainfall

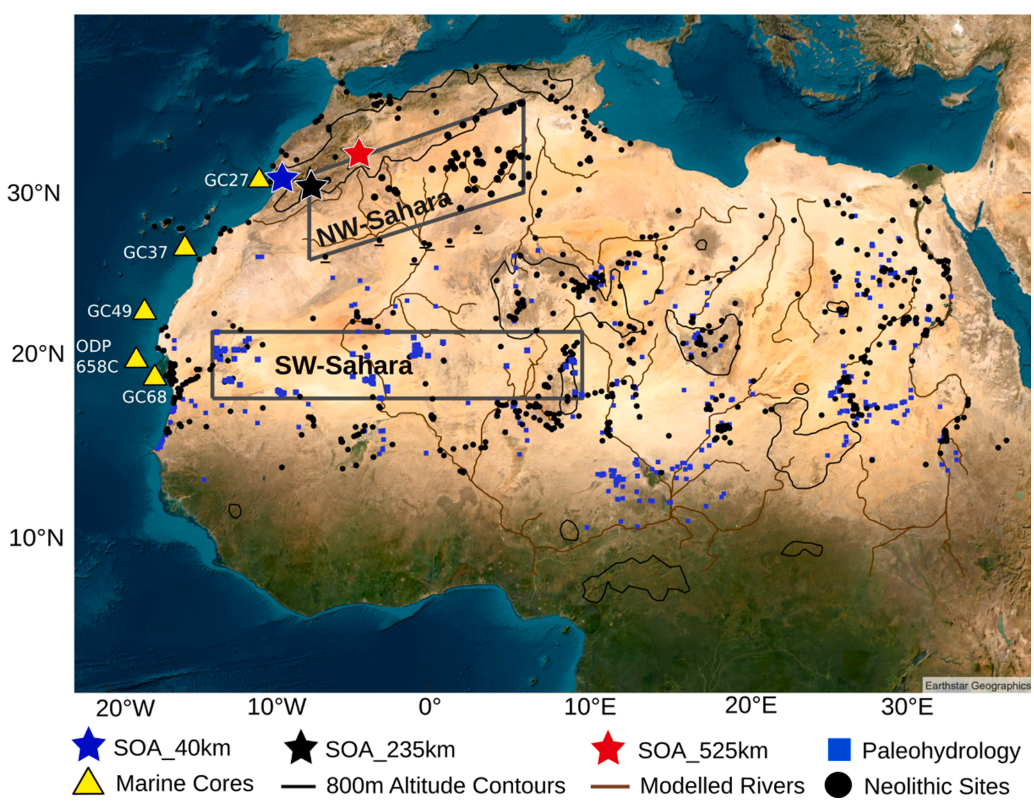

Fig. 1. Satellite image of North Africa, with NW-Sahara and SW-Sahara regions (grey boxes) used to compare the timing of increased-rainfall, surface hydrology, and archaeology. Black and red stars: study areas SOA_235km and SOA_525km from this work (four caves across two sites). Blue star: Wintimdouine cave record (SOA_40km) (Sha et al., 2019). Yellow triangles: dust flux or leaf wax isotope records from marine cores ODP-658C (Adkins et al., 2006), and GC68, GC49, GC37, GC27 (Tierney et al., 2017; McGee et al., 2013). Black lines: 800 m altitude contours. Brown lines: topographically-defined surface water flows modelled by this study using NASA SRTM3 data and Topotoolbox2 (Schwanghart and Scherler, 2014). Black dots: radiocarbon dated Neolithic sites compiled by (Manning and Timpson, 2014). Blue squares: radiocarbon dated surface hydrology records compiled by (Lézine et al., 2011).

from sites close to the north-western boundary of the Sahara (Fig. 1, box 'NW-Sahara', ∼30°N). There are complimentary speleothem records from Wintimdouine cave, at a near identical latitude to our sites, 30–40 km inland from the Atlantic coast. Growth is reported at Wintimdouine cave within Holocene, MIS2 and MIS5a time periods (Sha et al., 2019; Ait Brahim et al., 2023). Our new speleothem records, from ∼235 km and ∼525 km inland, are more shielded from North Atlantic and Mediterranean winter-rainfall by the High-Atlas mountains. There is no topographic barrier between South-of-Atlas cave sites and southern sources of rainfall (Fig. 1), ensuring that all can record periods of increased, southern-sourced rainfall. Modern-day TP rainfall supplies a small amount of rainfall at these South-of-Atlas sites (Knippertz, 2003).

We compare our new stalagmite palaeo-rainfall reconstructions with nearby records (Wintimdouine cave (Sha et al., 2019; Ait Brahim et al., 2023), Lake Tislit (Cheddadi et al., 2021)), with 183 palaeo-hydrology records from lakes and rivers (Lézine et al., 2011) from the south-west Sahara (Fig. 1, box 'SW-Sahara', ∼20°N), and with a meridional transect of palaeoclimate records between 19°N - 34°N (Adkins et al., 2006; Tierney et al., 2017; McGee et al., 2013; Ait Brahim et al., 2019; Wassenburg et al., 2016). We also compare our measured isotopes with the temperature difference between the extra-tropics (poleward of 30°) of the Northern and Southern Hemisphere, relative to a modern reference period, from hereon 'N-S temperature anomaly'. This N-S temperature anomaly is calculated using the regularised expectation-maximisation reconstructions (RegEM) algorithm (Marcott et al., 2013) with 73 globally distributed temperature records (Schneider et al., 2014), as is shown in Fig. 3a of Kaufman et al. (2020), with further detail in our supplementary material. These comparisons with wider regional processes are made to better assess the sources and controls of rainfall in the NW-Sahara and beyond.

2. Methods

2.1. Cave sites and sample descriptions

We report on four stalagmite samples from three caves at two sites located south-east of the Atlas mountains, ≥ 235 km inland from the Atlantic coast (Fig. 1).

Kef Thaleb and Asdif caves are within ∼10 km of each other in the Anti-Atlas Mountains (south of the Atlas mountains at 30°N, 7°W), ∼235 km inland from the Atlantic coast (black star, Fig. 1), with this area called SOA_235km from now on. Asdif and Kef Thaleb each have a single, small entrance, with little overlying bedrock (2–3 m Asdif, ∼5–30 m Kef Thaleb), wet cave sediments in the modern-day and evidence of more extensive water pools in the past. The modern day Köppen climate classification of the SOA_235km area is Cs, (mild temperate with dry summer). Modern-day rainfall patterns for all sites are summarized below (Section 3.2). Soil development above the caves is thin, with irregular coverage, and vegetation is sparse, with vegetation amount impacted by grazing. Stalagmites ASD-1, KFT-1 and KFT-3 are aragonite stalagmites from Asdif and Kef Thaleb caves respectively.

Ksar cave (red star, Fig. 1) is in the southernmost foothills of the High Atlas Mountains (32°N, 4°W), ∼525 km inland from the Atlantic coast. We refer to this location as the SOA_525km area. This cave was accessed via a small tunnel-shaped entrance. The overlying bedrock was ∼50m. Low cave ventilation and evidence of past water-pooling help to maintain high-humidity levels that are beneficial for oxygen isotope records. The modern day Köppen climate classification for the SOA_525km area is BW (desert arid). Modern-day vegetation is sparser at SOA_525km compared with SOA_235km. Stalagmite MM from Ksar cave is of calcite mineralogy.

Conditions were too dry at both of our SOA_235km and SOA_525km cave sites to allow for water collection during our work in the caves. Annotated images of all samples are available in the supplementary material.

Cave altitudes, in meters above sea level (masl), are near-identical for Ksar (1380 masl), Kef Thaleb (1380 masl) and Wintimdouine caves (1250 masl). Only Asdif cave from the SOA_235km region is higher (1880 masl).

2.2. XRD analysis

To verify the mineralogy of our speleothem material, aliquots of milled carbonate powders of ∼0.25 mg were analysed for XRD at the University of Oxford, Department of Earth Sciences, using a Panalytical Empyrean Series 2 powder diffractometer. HighScore software was subsequently used to detect peaks and calculate % of minerals based on user-selected best fit mineral candidates. MM was shown to be high-magnesium calcite, KFT-1, KFT-3 and ASD-1 are aragonite, in agreement with visible aragonite needles.

2.3. Stable isotope ratios: Stalagmite and rainfall values

Carbonate samples were milled along the growth axis of stalagmites ASD-1, KFT-1, KFT-3 and MM using a New Wave Micromill (for ASD-1, KFT-1, KFT-3), and an in-house macro-mill (for MM). In total, 702 samples were analyzed for oxygen and carbon stable isotopes using a Thermo-Scientific Delta V isotope ratio mass spectrometer (IRMS) coupled to a Kiel IV (for ASD-1, MM) or a GasBench II (for KFT-1, KFT-3) carbonate device at the University of Oxford, Department of Earth Sciences. All sample measurements were calibrated with NBS-18 and NBS-19 bracketing standards. All samples were reacted with 100 % H_3PO_4 at 71 °C.

The relative $^{18}O/^{16}O$ values are reported in the conventional $\delta^{18}O$ (‰) notation, relative to VPDB, on a normalised scale such that the $\delta^{18}O$ of NBS-19 is −2.2 ‰. Accuracy and precision were checked using a secondary standard's long-term average, included in all runs, with standard deviations of $\delta^{18}O = 0.07$ ‰ and $\delta^{13}C = 0.05$ ‰ (1σ).

For measurements of aragonite $\delta^{18}O$, IUPAC guidelines were followed to account for the difference in acid fractionation factor applicable to the calcite bracketing standards (NBS-18 and NBS-19) and the aragonite samples. We used aragonite acid fractionation factors from Kim et al. (2007), calcite acid fractionation factors from Kim et al. (2015), and the method/software of Kim et al. (2015) for normalising the stable isotope data of these two different carbonate mineralogies.

To directly compare the oxygen isotopes of aragonite and calcite stalagmite samples, a correction of −0.81 ‰ was applied to all $\delta^{18}O_{aragonite}$ values, to account for the difference in fractionation factor between aragonite and calcite mineralogies when precipitating from rain sourced water (Fohlmeister et al., 2018).

For rain oxygen isotopes ($\delta^{18}O_{rain}$), Global Network of Isotopes in Precipitation (GNIP) stations are not present in the South-of-Atlas region, and the semi-arid to arid climate hinders measured assessments. We use the Online Isotopes in Precipitation Calculator (OIPC) for average monthly rainfall $\delta^{18}O_{rain}$. We assess the overall validity of those calculated values by comparison with measurements of $\delta^{18}O_{rain}$ from Ait Brahim et al. (2019) (Fig. S1). Measured tropical-plume rainfall $\delta^{18}O_{TP\text{-}rain}$ is from Cappy (2007). All $\delta^{18}O_{rain}$ is expressed in ‰ relative to VSMOW. Calculated-$\delta^{18}O_{calcite}$ values are based on OIPC $\delta^{18}O_{rain}$, the calcite-water fractionation factor from Kim and O'Neil (1997), and a temperature of 16.5 °C based on the average temperature from measurements at Wintimdouine cave (Ait Brahim et al., 2019), which is at a very similar altitude to Kef Thaleb (SOA_235km) and to Ksar cave (SOA_525km).

2.4. U-Th chronology of stalagmite growth and age model

Absolute chronology of periods of speleothem-growth was conducted on milled carbonate powders from distinct growth laminae within six stalagmites. The milled carbonate powders were dissolved in distilled nitric acid and spiked with a $^{229}Th-^{236}U$ solution. The U and Th fractions were separated following chemical procedures from Edwards et al.

(1987). U and Th isotopes were measured separately using a Nu Plasma multi-collector inductively coupled plasma mass spectrometer (MC-ICP-MS) at the University of Oxford, Department of Earth Sciences, following the procedures described in Carolin et al. (2019). For correction of any initial, detrital Th, we used an initial $^{230}Th/^{232}Th$ ratio range of 0.2 to 16.8 ppm (activity 0.04 to 3.11), following a uniform distribution. The range of the initial $^{230}Th/^{232}Th$ ratio applied here (activity 0.04 to 3.11) for the initial ^{230}Th correction was determined using the stratigraphical constraint method. Aragonite stalagmites ASD-1, KFT-1 and KFT-3 have large sample (230/232), with small initial detrital ^{230}Th correction on the order of < 10 years (2s). Lower-uranium concentration stalagmite MM (calcite) has (230/232) values < 200, with correspondingly larger initial-Th correction (50–400 years (2s), depending on the sample). All ages were corrected to the year 1950 C.E (i.e., BP).

OxCal Version 4.3 was used to develop the age models for each stalagmite (Ramsey, 2009). The age models with 95 % confidence intervals were produced using the P-Sequence Poisson-process deposition model [k0 = 1 cm−1, log10 (k/k0) = U (−2,2)], defined by parameter k, which constrains the number of potential growth-rate changes per unit length (Ramsey and Lee, 2013). K0 was set to 1.

2.5. Defining areas 'NW-Sahara' and 'SW-Sahara' and the timing of increased surface-water within them

To compare the timing of speleothem growth at our sites with the timing of periods of northwards expansion of the WAM, we define two areas: i) a north-west Saharan region (28–32°N, 'NW-Sahara') applicable to our new stalagmite records; and (ii) a south-west Saharan region (18–22°N, 'SW-Sahara') (grey boxes, Fig. 1). Both areas are west of 10°E, to avoid eastern or Mediterranean sources of moisture. Both areas have hot desert climates in the modern-day (BWh Koppen climate classification), that are only likely to support speleothem growth or increased surface-water features as/when there is a distinct increase in rainfall levels compared with the present-day. The SW-Sahara area (18–22°N) is geographically close to the West African Monsoonal system (WAM). Strong proxy evidence supports the idea of insolation-driven, northward-migrations of monsoonal rainfall into the SW-Sahara area in the past (Gasse, 2000; Dallmeyer et al., 2020; Hely et al., 2014).

Due to a paucity of palaeohydrology records in the NW-Sahara we use the U-Th chronology of speleothem growth from this study, and the time-distribution of radiocarbon-dated artefacts from archaeological sites (Manning and Timpson, 2014) to assess the timing of wet periods in this area. In the SW-Sahara we use the compilation of terrestrial palaeohydrology studies by Lézine et al. (2011), and the time-distribution of radiocarbon-dated artefacts from archaeological sites compiled by Manning and Timpson (2014). In both the NW-Sahara and the SW-Sahara, the number of palaeohydrology and/or archaeology records are grouped into 500-year time windows, with ages expressed in years BP as reported in the original manuscripts (Lézine et al., 2011; Manning and Timpson, 2014).

2.6. Modern-day rainfall amounts

Modern-day data of rainfall-patterns for sites that feature heavily in our discussion, and data for the wider North African region are from Global Historical Climatology Network-Monthly stations (GHCN-M) and the KNMI Climate Explorer (Trouet and Van Oldenborgh, 2013). For our SOA_235km caves we use ERA-5 reanalysis data instead (Hersbach et al., 2020) because of differences in altitude between SOA_235km and the Ouarzazate GHCN-M site closest to SOA_235km.

3. Results

3.1. Timing and abundance of Holocene hydrological and archaeological records from SW-Sahara and NW-Sahara

The number of SW-Sahara palaeohydrology records increases sharply from 11 kyr BP, creating a single peak in the number of SW-Sahara records (10.5–7.5 kyr BP), which overlaps with the maximum in 20°N boreal summer insolation (JJA) (Fig. 2B). Subsequent to the 10.5–7.5 kyr BP peak there is a significant decrease in evidence for surface-water at ~7.5 kyr BP, and a further large decrease at ~5 kyr BP (Fig. 2B). There is complexity to the distribution of archaeology records in the SW-Sahara (Fig. S3), with multiple peaks centred on 9.5 kyr BP, 5.0 kyr BP, and 3.0 kyr BP.

In the inland NW-Sahara, all but four of our stalagmite U-Th ages (89 %) fall within the 8.7–4.3 kyr BP period (Fig. 2A). The four remaining ages (all < 1.1 kyr BP) are from stalagmite KFT-3, from the SOA_235km caves, evidence of resumed growth of stalagmite KFT-3 in the last millennium. Of the 160 Holocene radiocarbon ages from Neolithic sites in NW-Sahara, 80 % fall within the same 8.7–4.3 kyr BP period that includes 89 % of our speleothem U-Th ages. There is agreement between the rise and fall of the number of dated archaeological artefacts and the rise and fall of the N-S temperature anomaly curve (Fig. 2A), cf. Section 1 and supplementary material for full details on the anomaly curve.

During the early- to mid-Holocene, the average vertical extension rates of SOA_525km stalagmite MM is 29 um/year. The average vertical extension rate of SOA_235km stalagmites KFT-1, KFT-3, ASD-1 are 154 um/year, 95 um/year and 83 um/year respectively. Over the last ~1kyr BP, at site SOA_235km the average vertical extension rate of stalagmite KFT-3 is 88 um/year. There is variability in these vertical extension rates, ranging from 16 to 429 um/year, with regular darker colour banding in e.g. KFT-1 (Fig S7) suggestive of slowed/interrupted growth. For KFT-1 banding occurs at ~ 7kyr BP, 6.6 kyr BP, 6.5 kyr BP, 6.2 kyr BP, 5.8 kyr BP, 5.4 kyr BP. At the ~17 °C temperature of these caves the theoretical vertical extension rates are significantly higher, ~400–1410 um/year for solution calcium concentrations of 2–6 mmol/L (Baker et al., 1998).

Overall, evidence of increased surface-moisture begins at least 2 kyr earlier in the SW-Sahara than the NW-Sahara, and ends ~700 years earlier in the SW-Sahara (5 kyr BP) than in the NW-Sahara (4.3 kyr BP) (Fig. 2).

3.2. Modern-day patterns of rainfall, and of rainfall oxygen isotopes, at south-of-Atlas sites

South of the Atlas mountains, average annual rainfall in the modern-day decreases systematically with distance inland from the Atlantic coast: 234 mm/year for the Taroudant GHCN-M station (SOA_40km area), 158 mm/year for our SOA_235km cave sites, and 125 mm/year at our SOA_525km cave sites (Fig. S2). Decreased winter rainfall is primarily responsible for the inland reduction in annual rainfall-amount: i) 124 mm average winter rainfall for Taroudant (SOA_40km); ii) 51 mm for our SOA_235km cave sites; iii) 26 mm for our SOA_525km cave site. This causes a larger proportion of non-winter rainfall inland from the coast: 47 %, 67 %, 78 % of rainfall occurs in March-November for locations SOA_40km, SOA_235km, SOA_525km respectively. There is very little summer rainfall at any of these sites, an average total of 8 mm for months June, July and August (Fig. S2).

For all three regions (SOA_40km, SOA_235km, SOA_525km), there is a significant variation of OIPC modelled $\delta^{18}O_{rain}$ between months (~7 ‰) (Fig. S1). The impact of differences in site-altitude, or distance-from-coast, on $\delta^{18}O_{rain}$ is considerably smaller, < 2 ‰ in all cases (Fig. S1). The lowest modelled oxygen isotopes occur during the wettest six months (Oct, Nov, Dec, Jan, Feb, Mar), with average $\delta^{18}O_{rain}$ ~ −7.0 ‰ (Fig. S1). From GNIP observation data there are not significant differences between weighted annual $\delta^{18}O_{rain}$ from stations within the

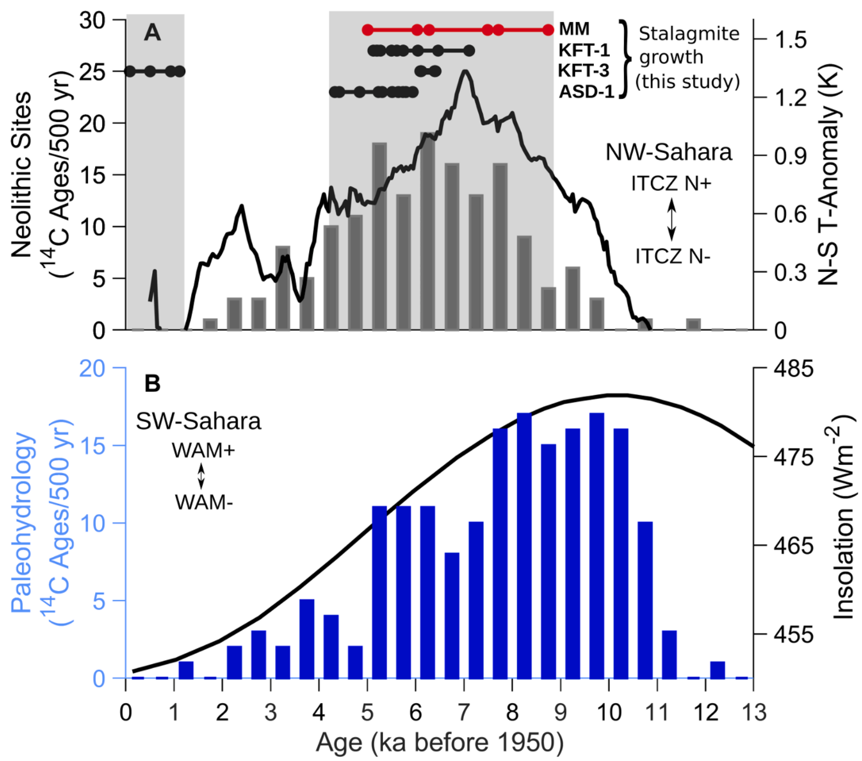

Fig. 2. Timing and abundance of paleo-environmental and archaeological records from NW-Sahara and SW-Sahara (grey boxes Fig. 1, Fig. 6). **(A)** New stalagmite records (this study) and archaeology from NW-Sahara. Red, black dots are new U-Th ages from stalagmite samples MM, KFT-1, KFT-3, ASD-1. Grey bar charts: number of ^{14}C ages (in 500-year bins) from Neolithic archaeological sites (Manning and Timpson, 2014) in NW-Sahara. Black curve: North-South inter-hemispheric temperature anomaly (Schneider et al., 2014); **(B)** Paleo-hydrology and insolation from SW-Sahara. Blue bar charts: number of paleo-hydrology records (in 500-year bins) from Lézine et al. (2011). Black line: 20°N June-August insolation curve, calculated with Berger and Loutre (1991), Huybers (2006).

Atlantic climate zone (with dominant Atlantic winter rainfall) and weighted annual $\delta^{18}O_{rain}$ from stations within the Mediterranean climate zone (with dominant Mediterranean winter rainfall) (Fig. 4B). For the driest six months (Apr, May, Jun, Jul, Aug, Sep), modelled $\delta^{18}O_{rain}$ is significantly higher, with average $\delta^{18}O_{rain}$ ~ −4.6 ‰, and values peaking in July at ~ 1.6 ‰. For the SOA_40km site, Ait Brahim et al. (2019) provides much-needed measured-$\delta^{18}O_{rain}$. There is encouraging agreement between measured-$\delta^{18}O_{rain}$ from Ait Brahim et al. (2019) and modelled OIPC $\delta^{18}O_{rain}$. Measured $\delta^{18}O_{rain}$ values also have large differences between the wet and dry seasons (~6–7 ‰). Some measured-$\delta^{18}O_{rain}$ in the drier months is several ‰ higher than modelled-$\delta^{18}O_{rain,}$ perhaps reflecting evaporative effects that are not accounted for by the modelled-$\delta^{18}O_{rain}$.

South-of-Atlas occurrences of TP-rainfall events have been shown to deliver up to 77 mm of rainfall in 24 h (e.g. Cappy, 2007; Knippertz et al., 2003). A common feature of these rainfall events is air masses travelling to the South-of-Atlas from the south, sometimes with vapour originating from < 10°N. These reported cases of TP-rainfall, with $\delta^{18}O_{rain}$ measurements, have heavily depleted oxygen isotopes (Cappy, 2007). Events in Dec 2002, October 2003 and October 2004 have $\delta^{18}O_{rain}$ of −15 ‰, −12 ‰, −12 ‰ respectively (average −13 ‰) (Cappy, 2007).

3.3. Modern speleothem and rainfall oxygen isotopes

Modelled top ages of stalagmites KFT-3 (SOA_235km) and WIN-2 (SOA_40km) are within uncertainty of modern, with KFT-3 sampled from an actively dripping part of the cave. There is agreement between 'measured-$\delta^{18}O_{calcite}$' from the top of these samples and 'calculated-$\delta^{18}O_{calcite}$' from weighted OIPC-modelled $\delta^{18}O_{rain}$ of the six wettest months (Oct, Nov, Dec, Jan, Feb, Mar). For KFT-3, measured-$\delta^{18}O_{calcite\text{-}KFT\text{-}3}$ ~ −7.2 ‰, calculated-$\delta^{18}O_{calcite\text{-}KFT\text{-}3}$ for the 6 wettest months ~ −7.5 ‰, calculated-$\delta^{18}O_{calcite\text{-}KFT\text{-}3}$ for annual rainfall ~ −6.6 ‰. For WIN, measured-$\delta^{18}O_{calcite\text{-}Win}$ ~ −7.0 ‰, calculated-$\delta^{18}O_{calcite\text{-}Win}$ for the 6 wettest months ~ −7.4 ‰, calculated-$\delta^{18}O_{calcite\text{-}Win}$ for weighted annual rainfall ~ −7.1 ‰. Using alternative oxygen isotope fractionation factors by Tremaine et al. (2011) instead of by Kim and O'Neil (1997) increases calculated-$\delta^{18}O_{calcite}$ by ~1 ‰.

3.4. Speleothem sample oxygen isotopes

Throughout its Holocene period of growth (~ 9–5 kyr BP), stalagmite MM from the SOA_525km region has consistently low $\delta^{18}O_{calcite}$ (average −9.9 ‰), with large short-term variability ($\delta^{18}O_{calcite}$ 1σ = 0.6 ‰) caused by regular ~2 ‰ shifts in $\delta^{18}O_{calcite}$ on centennial timescales (Fig. 3).

Oxygen isotopes from our SOA_235km cave stalagmites are highest during the last millennium (~ −7 ‰) and lowest at ~7 kyr BP (~ −11.5 ‰). The 7 kyr BP low point in $\delta^{18}O_{SOA\_235km}$ is coeval with the Holocene's maximum N-S hemisphere temperature difference anomaly. Oxygen isotopes from SOA_235km stalagmites decrease until this low point (~7 kyr BP), then increase until ~4.3 kyr BP ($\delta^{18}O_{SOA\_235km}$ ~ −8 ‰), when growth ceases (Fig. 3).

Stalagmite KFT-3 (from Kef Thaleb in the SOA_235km region) has a short ~300 year period of growth at ~6.2 kyr BP, and resumes growth between ~1–0 kyr BP. There is no long-term change in the $\delta^{18}O$ of KFT-3 during this period. Stalagmite KFT-3 $\delta^{18}O_{calcite}$ measurements are higher during the last millennium (average −6.7 ‰) compared with the mid-Holocene. For the whole of the last millennium KFT-3 and Wintimdouine $\delta^{18}O_{calcite}$ overlap (Figs. 4, 5). Stalagmite oxygen isotopes from SOA_235km and SOA_525km sites (~300 km apart) overlapped for >2 kyr between ~7.3–5 kyr BP.

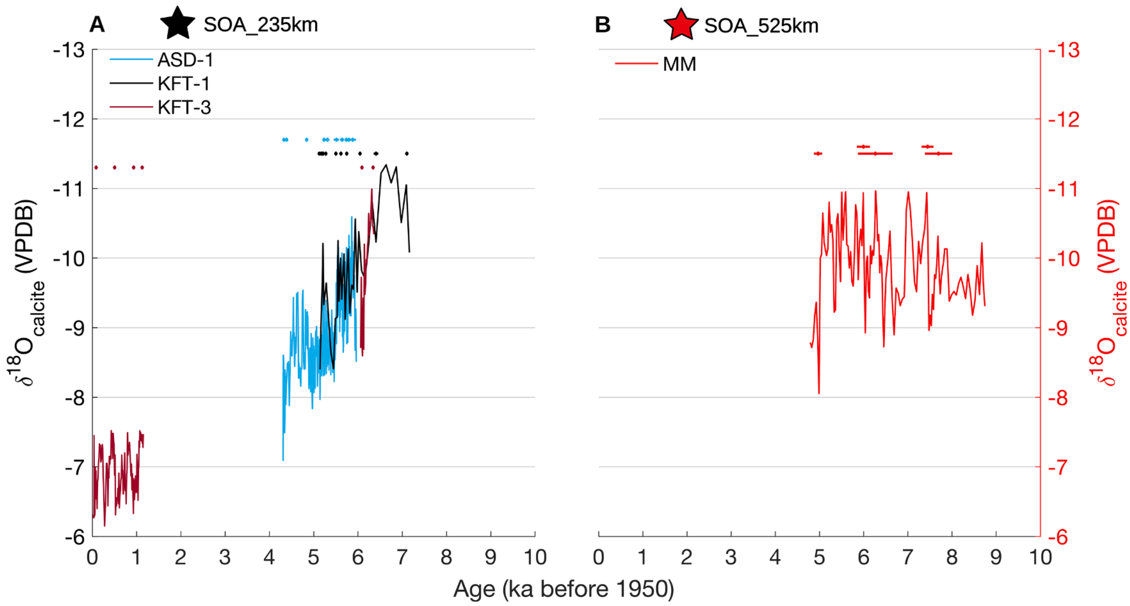

Fig. 3. Oxygen isotope results and U-Th chronology from all of our South-of-Atlas Holocene stalagmite samples. To directly compare the oxygen isotopes of aragonite and calcite samples, a correction of −0.81 ‰ was applied to all $\delta^{18}O_{aragonite}$ values, to account for the difference in fractionation factor between aragonite and calcite mineralogies when precipitating from rain sourced water (Fohlmeister et al., 2018). (A) SOA_235km stalagmites ASD-1, KFT-1, KFT-3 from ~235 km inland. (B) SOA_525km stalagmite MM from ~525 km inland.

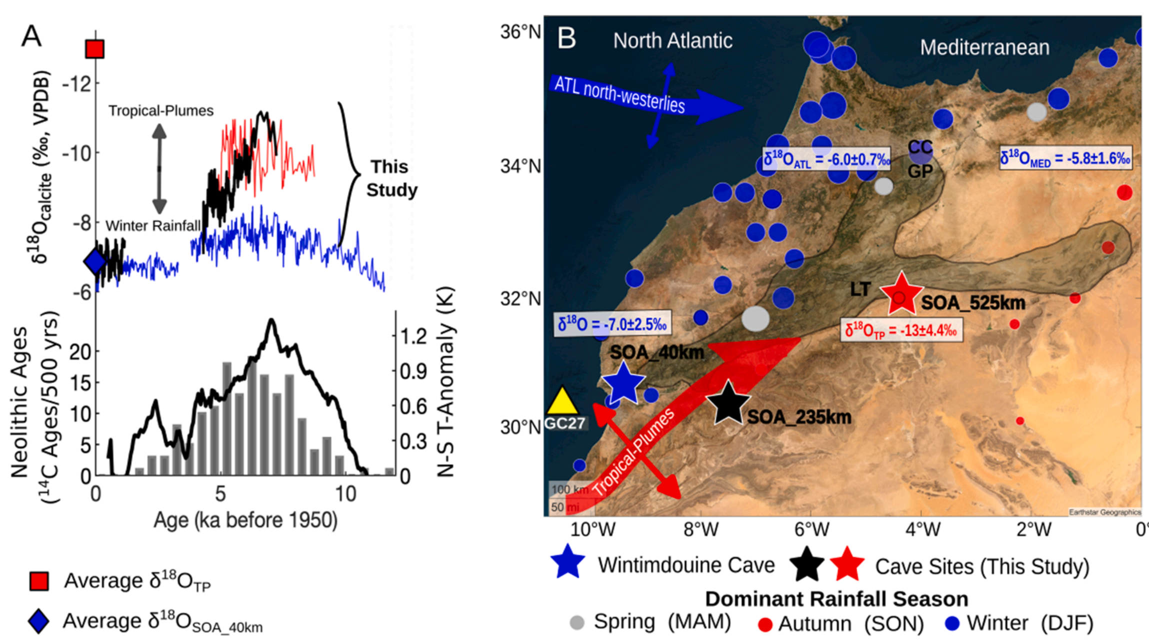

Fig. 4. Morocco stalagmite oxygen isotopes responding to tropical-plume (TP) rainfall-amount. Red, black, blue colours denote correspondence between isotope values (subplot A) and site locations (subplot B). **(A)** Red line ($\delta^{18}O_{SOA\_525km}$): new 'MM' stalagmite oxygen isotopes from inland site SOA_525km, with minimum winter rainfall. Blue line ($\delta^{18}O_{SOA\_40km}$): stalagmite oxygen isotopes from Wintimdouine cave (Sha et al., 2019) site SOA_40km. Upper black line ($\delta^{18}O_{SOA\_235km}$): new stalagmite oxygen isotopes from SOA_235km stalagmites (ASD-1, KFT-1, KFT-3), midway between SOA_40km and SOA_525km sites), with Holocene oxygen isotopes falling between values dominated by TP-sourced rainfall (red square) and Atlantic sourced rainfall (blue diamond). Lower black line: North-South hemisphere temperature anomaly from Schneider et al. (2014). **(B)** Locations of records $\delta^{18}O_{SOA\_525km}$ (red star), $\delta^{18}O_{SOA\_40km}$ (blue star) and $\delta^{18}O_{SOA\_235km}$ (black star). Circles and arrows are the same as in Fig. 6 (modern rainfall characteristics from GHCN-M sites, and schematic representation of TP-rainfall and Atlantic north-westerly trajectories). LT, CC, GP denote locations of Lake Tislit, Charaa Cave and Grotte de Piste records respectively (Cheddadi et al., 2021; Ait Brahim et al., 2019; Wassenburg et al., 2016).

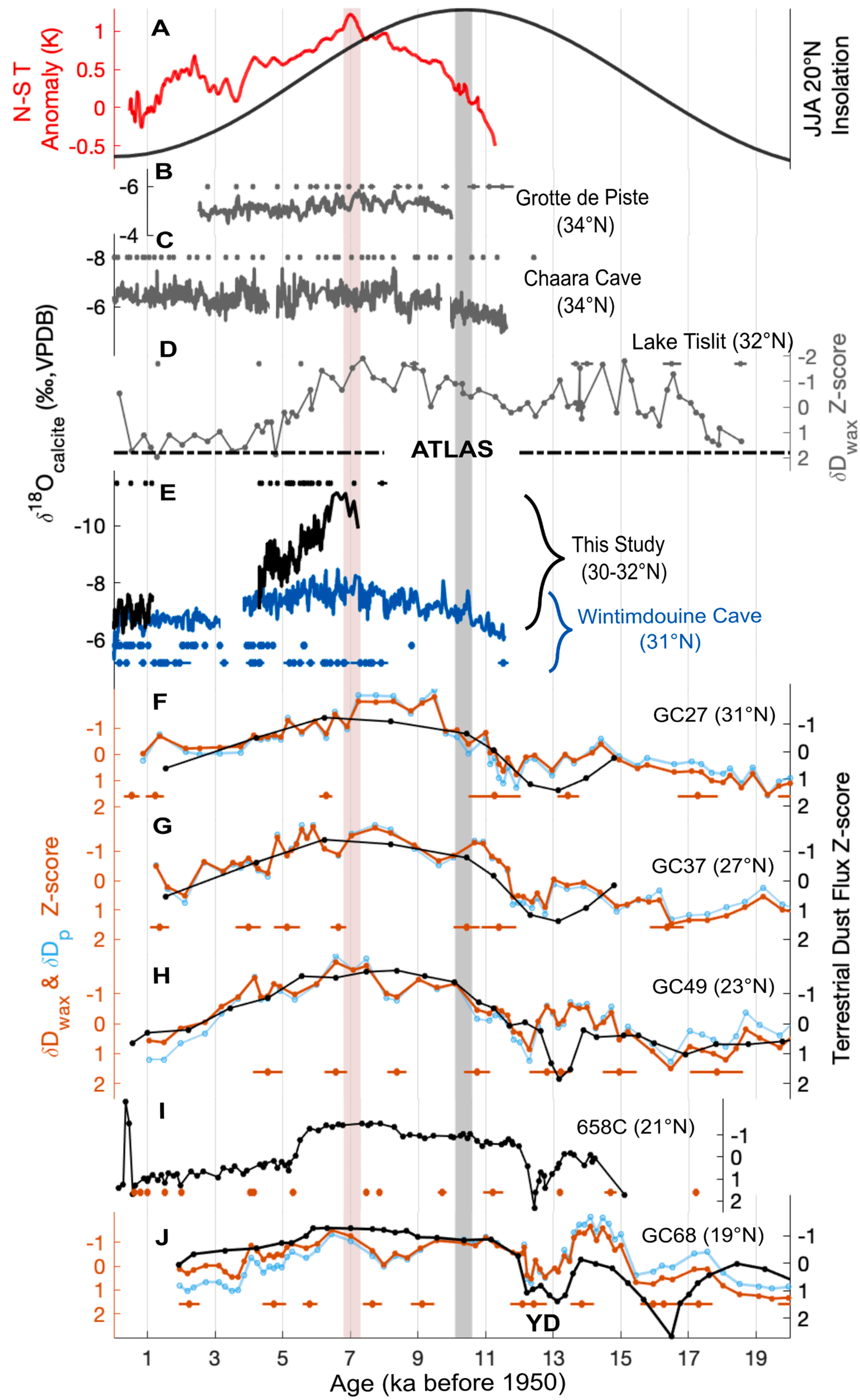

Fig. 5. Compilation of stalagmite, marine core and lake paleo-records between 19°N and 34°N. Records are ordered from North (top) to South (bottom). Thick, black dashed line: approximate representation of the position of the Atlas relative to the records. (A) N-S temperature anomaly (red) from Schneider et al. (2014), and 20°N June-August insolation curve (black), calculated with Berger and Loutre (1991), Huybers (2006). (B) stalagmite $\delta^{18}O$ from Grotte de Piste (Wassenburg et al., 2016) (C) $\delta^{18}O$ from stalagmite Cha1 from Chaara Cave (Ait Brahim et al., 2019). (D) Lake Tislit δD_{wax} Z-scores (Cheddadi et al., 2021). (E) Stalagmite $\delta^{18}O$ from this study and from Sha et al. (2019). (F, G, H, J) For marine cores GC27, GC37, GC49, GC68, Z-scores of terrestrial dust fluxes (black) from (McGee et al., 2013), and of δD_{WAX} (red), δD_P (light blue) from Tierney et al. (2017). (I) For marine core ODP658C, Z-scores of terrestrial dust fluxes (black) from Adkins et al. (2006). 'YD' Younger Dryas. Dark (light) grey vertical bar denotes timing of maximum 20°N June-August insolation (N-S T-anomaly) plotted in A.

Stalagmites from Wintimdouine cave (SOA_40km) have the same general trend in $\delta^{18}O_{calcite}$ as our SOA_235km stalagmites, with lowest $\delta^{18}O_{calcite} \sim -8$ ‰ at ~7 kyr BP. But the SOA_40km stalagmite record changes by a maximum of 1–2 ‰, whereas the SOA_235km stalagmites change by 4–5 ‰ over the course of the Holocene.

4. Discussion

4.1. Chronological constraints on the processes driving northern Sahara rainfall

Based on the timing of the Holocene wet period in the NW-Sahara versus the timing of the wet period in the SW-Sahara, we suggest the need for an additional, non-monsoonal source of rainfall in the NW-Sahara. In the NW-Sahara our U-Th chronology provides evidence of mid-Holocene stalagmite growth until 4.9 kyr BP at site SOA_525km, and until 4.3 kyr BP at SOA_235km. At SOA_40km, mid-Holocene Wintimdouine cave stalagmite growth continued until 3.9 kyr BP (Fig. 4, and (Sha et al., 2019)). In all cases, $\delta^{18}O_{calcite}$ was more depleted before growth ceased compared with more recent growth. For SOA_235km, $\delta^{18}O_{calcite}$ was depleted by ~1.5 ‰ at 4.5 kyr BP compared with renewed growth since 1.1 kyr BP (Fig. 3). For SOA_40km, $\delta^{18}O_{calcite}$ was depleted by ~0.5 ‰ at 4.5 kyr BP compared to renewed growth since ~3.3 kyr (Fig. 4, or Fig. 3 of Sha et al. (2019)). Of significance here is that isotopically depleted $\delta^{18}O_{calcite}$ continued to form until ~4 kyr BP at 30°N, with the significance of the isotopic results discussed in Section 4.2 below.

In the SW-Sahara (~20°N), where there is strong evidence of insolation-driven, northerly-migrations of WAM rainfall into this area in the past (e.g. Dallmeyer et al., 2020; Kuhlmann et al., 2004), a sharp drop in the number of surface hydrology records happened at ~5 kyr BP (Fig. 2B). This occurred when local 20°N insolation dropped below 470 W/m^2 (Fig. 2B), as per earlier suggestions of this insolation cut-off point causing a switch from humid to arid conditions in sub-tropical North Africa (deMenocal et al., 2000). This suggests that increased WAM-rainfall in the SW-Sahara stopped before (at or before ~5 kyr BP) the end of increased levels of isotopically-depleted rainfall in the NW-Sahara (at ~4 kyr BP).

It is difficult to see how the WAM could be the source of increased rainfall in the NW-Sahara until ~4 kyr BP whilst not supplying increased rainfall in the SW-Sahara since ~5 kyr BP. It is the continuation of rainfall to later times in the NW-Sahara compared with the SW-Sahara, something that this article is showing, that makes it possible to argue for an additional, non-monsoonal, source of rainfall to the NW-Sahara at this time, and to argue for a tropical-plume source of increased-rainfall for the NW-Sahara region.

From our records, we cannot be as confident that the WAM did not contribute moisture to the sub-tropics earlier in the Holocene, when there was more abundant surface water in the SW-Sahara (Fig. 2). Marine core GC27 (31°N) and Lake Tislit (32°N) δD_{wax} records show a broad peak of isotopically-depleted values at ~9 kyr BP (Fig. 5), which could be caused by increased WAM- and/or TP-rainfall amount, or by limited chronology over that time interval (Fig. 5).

4.2. Tropical plumes as a source of increased-rainfall in the early- to mid-Holocene NW-Sahara

We suggest a tropical-plume source of increased mid-Holocene rainfall for the NW-Sahara region, a hypothesis supported by the transect of stalagmite isotope records from the coast (Sha et al., 2019) to 525 km inland (at ~31°N) (this study). The agreement in oxygen isotopes between multiple samples of a given region provides confidence in the ability of these stalagmites to record regional $\delta^{18}O$ (Fig. 3, Fig. 4). From modern-day calcite, the agreement between measured-$\delta^{18}O_{calcite}$ and $\delta^{18}O_{calcite}$ calculated from rain $\delta^{18}O$ is an important endorsement of the ability of these stalagmites to effectively record rainfall $\delta^{18}O$ (cf. Section 3.4 for calculation details including the temperature and fractionation factors). The three main types of rainfall (dry season, wet season, and TP-rainfall events) have sufficiently distinct isotopic compositions (−4.6 ‰, −7.2 ‰, −13 ‰ respectively) to assess past changes in the weighted amounts of these types of rainfall.

The significantly depleted $\delta^{18}O_{calcite}$ of our early- to mid-Holocene stalagmite-growth (4–5 ‰ lower than modern-day $\delta^{18}O_{calcite}$) can be explained by increased levels of isotopically depleted TP-rainfall (~ 5–6 ‰ lower than winter rainfall). With all other variables unchanged, an additional ~270 mm/year of TP-rainfall is sufficient to recreate the 7 kyr BP low in $\delta^{18}O_{calcite}$ recorded by our SOA_235km and SOA_525km stalagmites. This level of increased TP-rainfall would facilitate the 9–5 kyr BP growth of stalagmite MM, in a region (SOA_525km) that is likely too arid in the modern-day (126 mm/year rainfall) for stalagmite-growth (Vaks et al., 2010). The depleted $\delta^{18}O_{calcite}$ of stalagmite MM (average −9.9 ‰ VPDB) is in line with isotopically-depleted $\delta^{18}O_{TP\text{-}rain}$. Timing of the lowest $\delta^{18}O_{calcite}$ from the coastal Wintimdouine cave also occurs at ~7 kyr BP, suggesting increased levels of TP-rainfall also at coastal sites. The smaller reduction of $\delta^{18}O_{calcite\text{-}SOA\_40km}$ values (only ~1 ‰ lower at 7 kyr BP compared to modern) can be explained by what we propose is a higher ratio of winter- to TP-rainfall along the coast during the Holocene. The lack of a long-term trend in the SOA_525km $\delta^{18}O_{calcite}$ can be explained by a predominant contribution of TP-rainfall at this inland-site between 9 and 5 kyr BP, with only minor amounts of winter rainfall (e.g. 28 mm in the modern-day) having a minimal impact on $\delta^{18}O_{calcite}$.

The mechanism we propose for explaining increased South-of-Atlas TP rainfall-amount during the early- to mid-Holocene is a northwards shift of the ITCZ, providing a more accessible supply of convective moisture above the tropical north Atlantic. Northward shifts of the ITCZ are induced by warmer northern hemisphere temperatures relative to the southern hemisphere (N-S temperature anomaly) (Schneider et al., 2014). During the Holocene, the maximum N-S hemisphere temperature anomaly occurs at ~7 kyr BP (supplementary material), coincident with the minimum in $\delta^{18}O$ in speleothems from the SOA_235km and SOA_40km (Fig. 5D). From modern-day studies, the amount of rainfall transported by individual TPs is variable, responding to factors such as the amount of moisture in the 'tropical reservoir', and the degree to which equatorward troughs overlap (vertically and horizontally) with the tropical moisture reservoir (Knippertz, 2007). We hypothesize that a more northerly ITCZ increases the overlap and supply of convective moisture from the Atlantic-ITCZ to the upper-level troughs that carry tropical moisture northwards (Fig. 6). A close connection between the ITCZ and the origin of TP rainfall is noted by many studies (Thepenir and Cruette, 1981; Iskenderian, 1995; Mcguirk et al., 1987; Ziv, 2001). Of the 145 cloud bands studied by (Thepenir and Cruette, 1981), 101 have their cloud embryo within the ITCZ. Modern-day observations also indicate that northwards (southwards) shifts in the ITCZ result in increased (decreased) number of TPs (Knippertz, 2003), in agreement with the hypothesis we propose for the mid-Holocene.

Whilst we cannot provide detailed characterisation of the rainfall, features from all four of our stalagmites suggest modest increased-rainfall, in keeping with ~270 mm extra rainfall suggested from isotopic considerations. The low vertical extension rates (29–154 um/year, Section 3.1) are likely explained by in-cave dripping for only part of the year, arguing against abundant, year-round rainfall. Frequent abrupt shifts in oxygen isotopes (Fig. 3), variability in the vertical extension rates, and repeated dark banding (e.g. Fig. S6), which may indicate episodes of reduced/interrupted growth, are suggestive of variability in rainfall-delivery. This variability fits with modern-day observations of TPs, with their timing, trajectories and rainfall-amount changing dynamically through time (Section 1). Modest increases in rainfall-amount are in keeping with multiple modelling studies (e.g. Boateng et al., 2024; Hopcroft and Valdes, 2019; Shi et al., 2023).

Two palaeoclimate modelling studies based on MPI-ESM1.2 and CAM5 models also identify TPs as a source of increased rainfall in their 6

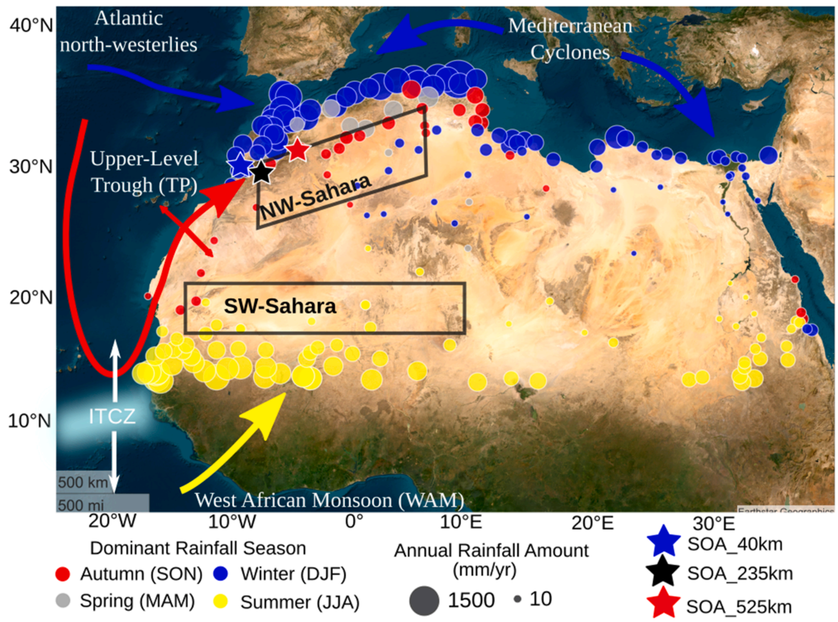

Fig. 6. Summary of modern-day North African rainfall. Rainfall data was selected from GHCN-M stations north of 14° N, with a minimum of 30-years of rainfall measurements, and without significant gaps in the data (Trouet and Van Oldenborgh, 2013). Rainfall is plotted as circles: size is proportional to annual rainfall amount (2 to 1500 mm/yr); colour denotes months with most rainfall. Most rainfall in June-August (yellow); September-November (red); December-February (blue); Mar-May (grey). Black and red stars: study areas from this work (four caves from two sites). Blue star Wintimdouine cave (Sha et al., 2019). Grey boxes 'NW-Sahara' and 'SW-Sahara', defined in this study to compare the timing of increased-rainfall, surface hydrology, and archaeology. Arrows: example, schematic representations of trajectories for WAM (yellow), Atlantic north-westerlies (blue), Mediterranean cyclones (blue), upper-level troughs (red). These arrows are example trajectories only, which can vary significantly between events. Light-blue shaded area 'ITCZ': current average position of boreal-summer Atlantic-ITCZ (Schneider et al., 2014), white arrows are a cartoon representation of migrations of this mean position through time.

kyr BP model output (MH) (Dallmeyer et al., 2020; Skinner and Poulsen, 2016). From Skinner and Poulsen (2016), averaged over 10°W-10°E at ~32°N, ~200–250 mm extra rainfall is predicted to have occurred at 6 kyr BP compared with pre-industrial (PI), with the additional rainfall predicted for the boreal autumn months. Agreement between our speleothem-based hypothesis and model output is encouraging. Models are crucial for effective consideration of climate-dynamics complexity, e.g. consideration of both trough behaviour and the tropical sources of convective moisture. Both modelling studies (Dallmeyer et al., 2020; Skinner and Poulsen, 2016) suggest WAM derived surface-water as the main source of moisture causing additional TP-rainfall at 6 kyr BP. WAM derived surface-water supplying moisture for TP rainfall is unlikely to remain true after the SW-Sahara dries at ~5 kyr BP, with isotopically depleted rainfall persisting in the South-of-Atlas until ~4 kyr BP. Due also to a closer fit of South-of-Atlas $\delta^{18}O_{speleothem}$ with the N-S T-anomaly curve than with insolation we suggest that, in addition to WAM surface-moisture, N-S temperature anomalies and the position of the Atlantic-ITCZ influence TP-rainfall amount. In the modern-day, more than twice as many TP events originate over the Atlantic than over tropical Africa (Iskenderian, 1995), in support of this proposal.

A study of 20 years of meteorological records, with back-trajectory analysis of reanalysis data, suggests that many TP trajectories follow the West African Atlantic coast towards north-west Africa (Knippertz, 2003). Whilst not all TPs originate in the tropical north Atlantic ocean, and not all TP trajectories follow the coastline (e.g. example in Cappy, 2007), modern-day weather-station data shows that most of the annual coastal rainfall (between 20°N and 30°N) occurs during the autumn season (often associated with TP-rainfall), cf. red dots from this study Fig. 6, and red area Fig. 7 from Dallmeyer et al. (2020). Any increase in mid-Holocene TP-rainfall along the Atlantic coast could help to reconcile the South-of-Atlas speleothems and Atlantic coast marine cores having minimum isotope and TDF values at ~7 kyr BP (Fig. 5).

4.3. Comparing NW-Sahara speleothem records with palaeo-data and with suggested rainfall-mechanisms from the wider north west Africa region

We propose overall agreement between stalagmite, marine and lake records in this sub-tropical NW-Africa region. In all cases the minima ($\delta^{18}O_{stalagmite}$, total dust flux (TDF) and δD_{wax}) occurs at ~7 kyr BP, supporting the hypothesis of an increased amount of isotopically depleted rainfall at this time. Although our tropical-plume hypothesis differs from earlier interpretations.

Based on δD_{wax} Tierney et al. (2017) argued for WAM-rainfall reaching at least 31°N before retreating southwards, evidenced by δD_{wax} returning to higher values earlier in marine core GC27 (31°N) than in core GC37 (27°N). However, reduced dust fluxes (indicative of increased-rainfall) do not end earlier in GC27 than in GC37 (Fig. 5). And we present speleothem records also showing isotopically-depleted rainfall ending later in the NW-Sahara than in the SW-Sahara (Section 4.1).

Wintimdouine speleothem studies also argued for increased mid-Holocene WAM rainfall at 31°N (Sha et al., 2019; Ait Brahim et al., 2023) on the basis of Tierney et al. (2017), Pausata et al. (2016), and on expectation that increased WAM rainfall-amount caused the depleted mid-Holocene $\delta^{18}O_{speleothem}$. Modelling studies since Pausata et al. (2016) are less supportive of WAM-rainfall reaching 31°N (Hopcroft and Valdes, 2019; Pausata et al., 2020), and we argue against the WAM hypothesis of Tierney et al. (2017). There is limited consensus on whether sub-tropical WAM-rainfall was isotopically depleted. Isotope-enabled models show depleted $\delta^{18}O_{rain}$ for the South-of-Atlas MH relative to the PI, but neither are statistically significant (Boateng et al., 2024; Shi et al., 2023). Simulated depletions of $\delta^{18}O_{rain}$ (MH - PI) are smaller (−0.4 ‰ annual average depletion Shi et al., 2023) than required to explain 1–2 ‰ (4–5 ‰) depletions of SOA_40km (SOA_235km) $\delta^{18}O_{speleothem}$. For δD_{rain}, the simulated MH-PI for the Northwestern Sahara ranges from −1.3 ‰ (with desert-level vegetation) to +3.5 ‰ (with increased MH vegetation) (Thompson et al., 2021). Since Tierney et al. (2017), Sha et al. (2019) new Lake Tislit (32°N) palynology data suggests no increased JJA rainfall since 18,500 year BP (Cheddadi et al., 2021).

Winter rainfall from Atlantic north-westerlies (ANW) supplies rainfall to sites north of the Atlas, and to coastal sites immediately south of the Atlas mountains. The amount of ANW rainfall travelling inland, along the southern slopes of the Atlas is small, with only 28 mm of modern-day winter rainfall reaching our SOA_525km cave site. We do not expect increased ANW-rainfall, or a rainfall amount effect on oxygen isotopes, to explain the mid-Holocene depletion in $\delta^{18}O_{rain.}$ At monthly or seasonal timescales it is the number of storm events that controls winter rainfall amount, not rainfall convection. Based on long-term Global Network of Isotopes in Precipitation (GNIP) measurements at Fes-Sais, Morocco (1994–2021), there is no significant relationship between rainfall amount and $\delta^{18}O_{rain}$ for any of the winter months (Dec, Jan, Feb, p-values 0.6, 0.07, 0.6 respectively). Some previous studies suggest that winter rainfall in NW Africa was reduced in the mid-Holocene, with proxy evidence for a positive North Atlantic Oscillation phase, which shifts winter storm-tracks northwards, reducing winter rainfall events in north-west Africa (Sha et al., 2019; Ait Brahim et al., 2019; Repschläger et al., 2017).

Mediterranean winter cyclones extending south of the Atlas have also been proposed as an alternative source of moisture to the NW-Sahara area. Review work by Gasse (2000) suggested northern-sourced airmasses and rainfall reaching 25°N in extreme events, although Larrasoana et al. (2013) cautions that rainfall from these sources normally decreases rapidly to < 100 mm/year within 100–200 km of the coast, limiting their impact. The sediment record from Lake Tislit (Cheddadi et al., 2021) (Fig. 4B 'LT', Fig. 5D), in close proximity to our Ksar cave (Fig. 4 red star), is of key interest. Lake Tislit is at the topographical high-point between north and south of the Atlas. Based on their proposed pollen-based reconstruction of winter rainfall-amount (peaking between 10 and 9 kyr BP), and a minimum in δD_{rain} (derived from δD_{wax}) between 9 and 6 kyr BP, they propose a significant role of Mediterranean cyclones delivering rainfall south of the Atlas. They point to similarities between δD_{wax} from their lake sediments, and δD_{wax} from marine cores GC27 (31°N) and GC37 (27°N) to propose incursions of Mediterranean rainfall to between 18 and 24°N. However South-of-Atlas rain-derived isotopic records (≤ 32°N) have a different trend to those from north of the Atlas, e.g. from high-resolution, continuous Chaara and Grotte de Piste cave records at 34°N (Ait Brahim et al., 2019; Wassenburg et al., 2016). Grotte de Piste and Chaara caves, located 2° further north than Lake Tislit, closer to the Mediterranean cyclones and to the Mediterranean climate zone (Fig. 4, 'GP', 'CC'), have little long-term trend in $\delta^{18}O_{calcite}$, whereas Lake Tislit δD_{wax} has a low at ~7 kyr BP followed by a transition to significantly higher values (Fig. 5). An alternative hypothesis is that Lake Tislit δD_{wax} was also impacted by southern-sourced TP-rainfall. The isotopic depletion of TP-rainfall fits with the Lake Tislit δD_{wax} minima around 7 kyr BP. Increased autumn TP-rainfall also aligns with the increased autumn rainfall suggested by Lake Tislit reconstructed rainfall (calculated from data in Cheddadi et al., 2021).

In summary, there is strong agreement of our records of peak increased-rainfall centred around 7 kyr BP, with existing rain-controlled isotopes and TDF records. We suggest that TPs represent an important additional source of rainfall to the sub-tropical rainfall mix.

4.4. Holocene rainfall patterns: Archaeology implications

The precise location and the timing of increased rainfall levels made possible by these four new stalagmite records allows for a reassessment of the relationship between increased rainfall and human habitation in the NW-Sahara. An early, pioneering study into connections between North African demography and climate (Manning and Timpson, 2014) demonstrates the difficulty of interpreting archaeology and demography with insufficiently resolved environmental data. At the time of its publication, a lack of records and lack of recognition of the spatial heterogeneity of the loosely termed 'Saharan' climate allowed the authors of this early record to propose a thousand-year lag of demography relative to climate change. Here we demonstrate differences in the timing of wet periods within distinct regions of the western Sahara. Considering only locations in the NW-Saharan region of the dataset of Manning and Timpson (2014) indicates a strong agreement between periods of stalagmite growth and archaeology (Fig. 2A). Of the 160 Holocene Neolithic site radiocarbon (^{14}C) ages in this region, 80 % fall within the 8.7–4.3 kyr BP period of peak increased rainfall, suggesting that increased rainfall improved habitability within this region.

North-south Sahara connectivity is key to understanding the dispersal of human cultural influences from its centre in sub-Saharan Africa. To the north of sub-Saharan Africa, the Sahara impedes connections and exchanges. Periods of improved north-south connectivity across the western Sahara have been inferred from zoo-geographical evidence, including the trans-Saharan distribution of numerous aquatic species (Drake et al., 2011). Until now, however, there lacked certainty regarding the timing and spatial coverage of wetter conditions, particularly in the north-western desert. The timing of increased rainfall in the NW-Sahara relative to the SW-Sahara (Fig. 2) demonstrates a period of overlap of WAM increasing rainfall in the SW-Sahara and TP-rainfall increasing rainfall in the NW-Sahara. This suggests that particularly between ~8.7 kyr BP and 5 kyr BP there was a significant narrowing of the Sahara.

Enhanced rainfall in this NW-Sahara region recharged major aquifers and increased recharge to rivers flowing southwards into the Sahara (Heiß et al., 2020), cf. our topographically modelled rivers (Fig. 1) using TopoToolbox (Schwanghart and Scherler, 2014). Of the 15 radiocarbon ages at 7 archaeological sites directly south of the NW-Sahara (underlined black dots Fig. 1), 80 % of these ages also fall within the 8.7–4.3 kyr BP period, adding some support to the suggestion that rivers flowing south from the NW-Sahara could have improved habitability further south.

Improved habitability in NW-Sahara and SW-Sahara, increased recharge to NW-Sahara rivers flowing south into the Sahara, and a narrower desert may have facilitated connections, and encouraged movement, by people across the Sahara, during a key period in the development of land use and animal production (Broich et al., 2021; Dunne et al., 2018; Phelps et al., 2020).

5. Conclusions

This study contributes Holocene U-Th chronology and continuous oxygen isotopes records from four stalagmites that formed inland (30–32° N, 7–4° W) in the Moroccan South-of-Atlas region. Modern-day average annual rainfall at our sites (158 and 125 mm/year) is at or below the limit of what is expected for speleothem-growth. Only one of these stalagmites grew during the last millennium. All four stalagmites grew for hundreds to thousands of years between 8.7–4.3 kyr BP, with oxygen isotopes up to ~4 ‰ lower compared to 1.1–0.1 kyr BP. Minimum $\delta^{18}O_{stalagmite}$ occurs at ~7 kyr BP. We propose that an increase in the amount of isotopically-depleted Tropical Plume (TP) rainfall (~6–7 ‰ lower than winter rainfall) contributed to the growth of the four stalagmites between 8.7–4.3 kyr. We suggest that the amount of TP-rainfall increased as a result of the increase in the North-South inter-hemispheric temperature anomaly shifting the Atlantic-ITCZ northwards. The increased palaeo-rainfall supported an increase in the region's archaeological activity between 8.7–4.3 kyr BP. Improved habitability and increased recharge to rivers flowing south into the Sahara likely facilitated greater connectivity through the Sahara, during a key period in the development of land use and animal production.

Significance statement

Stalagmite palaeoclimate records from the north-western boundary of the Sahara (30–32° N, 4–7° W) provide new chronology for a period of increased-rainfall during the Holocene (8.7–4.3 kyr BP). The location, timing, and oxygen isotopes of the speleothem growth, in comparison with other records, strongly suggests that South-of-Atlas rainfall continued after the decline of the West African Monsoon (WAM) in the mid-Holocene. We suggest that tropical plumes increased the export of moisture to the subtropics during a period of increased temperatures in the Northern Hemisphere relative to the Southern Hemisphere. This tropical plume mechanism can deliver convecting moisture from the tropics (over the North-Atlantic, or from WAM-supplied terrestrial surface moisture) to the subtropics. Increased recharge to rivers flowing south into the Sahara as a result of this increased rainfall may have facilitated connections during a key period in the development of land use and animal production.

Classification

Physical Sciences. Earth, Atmospheric, and Planetary Sciences.

CRediT authorship contribution statement

Hamish O. Couper: Writing – original draft, Methodology, Investigation, Formal analysis, Data curation, Conceptualization. **Christopher C. Day:** Writing – review & editing, Writing – original draft, Visualization, Validation, Supervision, Project administration, Methodology, Investigation, Formal analysis, Conceptualization. **Julia J. Barrott:** Writing – original draft, Methodology, Investigation, Funding acquisition, Formal analysis, Data curation, Conceptualization. **Samuel J. Hollowood:** Writing – review & editing, Investigation, Formal analysis, Data curation. **Stacy A. Carolin:** Writing – review & editing, Methodology, Investigation, Formal analysis, Data curation. **Ben Lovett:** Investigation. **Abdeljalil Bouzouggar:** Resources, Project administration, Conceptualization. **Nick Barton:** Writing – review & editing, Validation, Supervision, Resources, Project administration, Funding acquisition, Conceptualization. **Gideon M. Henderson:** Writing – review & editing, Validation, Supervision, Resources, Project administration, Investigation, Funding acquisition, Conceptualization.

Declaration of competing interest

The authors declare that they have no known competing financial interests or personal relationships that could have appeared to influence the work reported in this paper.

Acknowledgments

We are grateful to the Institut National des Sciences de l'Archéologie et du Patrimoine (INSAP, Rabat, Morocco) for providing permission for this work. We thank the Boise Fund for supporting the DPhil project of Julia Barrott, and the fieldwork expedition. The DPhil project of Hamish Couper was supported by NERC—Oxford DTP project NE/L002612/1. We are grateful to Andrew Mason, Tom Browning, Alex Thomas and Alan Hsieh for their assistance with U-Th measurements, to Katherine Clayton for XRD measurements, to Owen Green for assistance with microscopy, petrography. We thank Gillian Hoyle and the Gordon Foundation for lending us a Land Rover fieldwork vehicle. We thank Matthew Setchfield, librarian of the Westminster Speleological Group, for assisting with library material for fieldwork planning. And we are immensely grateful for the generosity of many locals at our cave sites for providing local information and support. We are grateful for the editorial handling of our manuscript, for helpful reviewer input by Jasper Wassenburg, and for helpful anonymous reviewer input.

Supplementary materials

Supplementary material associated with this article can be found, in the online version, at doi:10.1016/j.epsl.2024.119195.

Data availability

Associated data has been uploaded in CSV format with this article

References

Adkins, J., deMenocal, P., Eshel, G., 2006. The "African humid period" and the record of marine upwelling from excess ^{230}Th in Ocean Drilling Program Hole 658C. Paleoceanography 21, 1–14. https://doi.org/10.1029/2005PA001200.

Ait Brahim, Y., Wassenburg, J.A., Sha, L., Cruz, F.W., Deininger, M., Sifeddine, A., Bouchaou, L., Spötl, C., Edwards, R.L., Cheng, H., 2019. North Atlantic ice-rafting, ocean and atmospheric circulation during the holocene: insights from western mediterranean speleothems. Geophys. Res. Lett. 46, 7614–7623.

Ait Brahim, Y., Bouchaou, L., Sifeddine, A., Beraaouz, E.H., Wanaim, A., Cheng, H., 2019. Hydro-climate characteristics of the karst system of Wintimdouine cave (Western High Atlas, Morocco): monitoring and implications for paleoclimate research. Environ. Earth Sci. 78, 508.

Ait Brahim, Y., Sha, L., Wassenburg, J.A., Azennoud, K., Cheng, H., Cruz, F.W., Bouchaou, L., 2023. The spatio-temporal extent of the Green Sahara during the Last Glacial Period. iScience, 107018.

Baker, A., Genty, D., Dreybrodt, W., Barnes, W.L., Mockler, N.J., Grapes, J., 1998. Testing theoretically predicted stalagmite growth rate with recent annually laminated samples: implications for past stalagmite deposition. Geochim. Cosmochim. Acta 62, 393–404.

Berger, A., Loutre, M.F., 1991. Insolation values for the climate of the last 10 million years. Quat. Sci. Rev. 10, 297–317.

Boateng, D., Aryee, J.N.A., Baidu, M., Arthur, F., Mutz, S.G., 2024. West African monsoon dynamics and its control on the stable oxygen isotopic composition of precipitation in the late cenozoic. J. Geophys. Res. Atmospheres 129 e2024JD040748.

Braconnot, P., Otto-Bliesner, B., Harrison, S., Joussaume, S., Peterchmitt, J.-Y., Abe-Ouchi, A., Crucifix, M., Driesschaert, E., Fichefet, T., Hewitt, C.D., Kageyama, M., Kitoh, A., Laîné, A., Loutre, M.-F., Marti, O., Merkel, U., Ramstein, G., Valdes, P., Weber, S.L., Yu, Y., Zhao, Y., 2007. Results of PMIP2 coupled simulations of the Mid-Holocene and Last Glacial Maximum - Part 1: experiments and large-scale features. Clim. Past 3, 261–277.

Broich, M., Potì, A., Linstädter, J., Gibaja, J.F., Mazzucco, N., Conesa, M.V., Mikdad, A., Weniger, G.-C., 2021. The early and middle holocene lithic industries of Ifri n'Etsedda (Eastern Rif, Morocco). Afr. Archaeol. Rev. 38, 49–71.

S. Cappy, Hydrogeological characterization of the Upper Drâa catchment: morocco. 41–68 (2007).

Carolin, S.A., Ersek, V., Roberts, W.H.G., Walker, R.T., Henderson, G.M., 2019. Drying in the middle east during northern hemisphere cold events of the early glacial period. Geophys. Res. Lett. 46, 14003–14010.

Cheddadi, R., Carré, M., Nourelbait, M., François, L., Rhoujjati, A., Manay, R., Ochoa, D., Schefuß, E., 2021. Early Holocene greening of the Sahara requires Mediterranean winter rainfall. Proc. Natl. Acad. Sci. 118.

Cremaschi, M., Zerboni, A., Spötl, C., Felletti, F., 2010. The calcareous tufa in the Tadrart Acacus Mt. (SW Fezzan, Libya): an early Holocene palaeoclimate archive in the central Sahara. Palaeogeogr. Palaeoclimatol. Palaeoecol. 287, 81–94.

Dallmeyer, A., Claussen, M., Lorenz, S.J., Shanahan, T., 2020. The end of the African humid period as seen by a transient comprehensive Earth system model simulation of the last 8000 years. Clim. Past 16, 117–140.

deMenocal, P., Ortiz, J., Guilderson, T., Adkins, J., Sarnthein, M., Baker, L., Yarusinsky, M., 2000. Abrupt onset and termination of the African Humid Period:: rapid climate responses to gradual insolation forcing. Quat. Sci. Rev. 19, 347–361.

Drake, N.A., Blench, R.M., Armitage, S.J., Bristow, C.S., White, K.H., 2011. Ancient watercourses and biogeography of the Sahara explain the peopling of the desert. Proc. Natl. Acad. Sci. U. S. A. 108, 458–462.

Dubief, J., Queney, P., 1935. Les grands traits du climat du Sahara Algérien. La Météorologie 81–91.

Dunne, J., di Lernia, S., Chłodnicki, M., Kherbouche, F., Evershed, R.P., 2018. Timing and pace of dairying inception and animal husbandry practices across Holocene North Africa. Quat. Int. 471, 147–159.

Edwards, R.L., Chen, J.H., Ku, T.-L., Wasserburg, G.J., 1987. Precise timing of the last interglacial period from mass spectrometric determination of thorium-230 in corals. Science (1979) 236, 1547–1553.

Fohlmeister, J., Arps, J., Spötl, C., Schröder-Ritzrau, A., Plessen, B., Günter, C., Frank, N., Trüssel, M., 2018. Carbon and oxygen isotope fractionation in the water-calcite-aragonite system. Geochim. Cosmochim. Acta 235, 127–139.

Gasse, F., 2000. Hydrological changes in the African tropics since the last glacial maximum. Quat. Sci. Rev. 19, 189–211.

Geen, R., Bordoni, S., Battisti, D.S., Hui, K., 2020. Monsoons, ITCZs, and the concept of the global monsoon. Rev. Geophys. 58.

Heiß, L., Bouchaou, L., Tadoumant, S., Reichert, B., 2020. Multi-tracer approach for assessing complex aquifer systems under arid climate: case study of the River Tata catchment in the Moroccan Anti-Atlas Mountains. Appl. Geochem. 120, 104671.

Hely, C., Lézine, A.-M., Contributors, A., 2014. Holocene changes in African vegetation: tradeoff between climate and water availability. Clim. Past 10, 681–686.
Hersbach, H., Bell, B., Berrisford, P., Hirahara, S., Horányi, A., Muñoz-Sabater, J., Nicolas, J., Peubey, C., Radu, R., Schepers, D., Simmons, A., Soci, C., Abdalla, S., Abellan, X., Balsamo, G., Bechtold, P., Biavati, G., Bidlot, J., Bonavita, M., De Chiara, G., Dahlgren, P., Dee, D., Diamantakis, M., Dragani, R., Flemming, J., Forbes, R., Fuentes, M., Geer, A., Haimberger, L., Healy, S., Hogan, R.J., Hólm, E., Janisková, M., Keeley, S., Laloyaux, P., Lopez, P., Lupu, C., Radnoti, G., de Rosnay, P., Rozum, I., Vamborg, F., Villaume, S., Thépaut, J.-N., 2020. The ERA5 global reanalysis. Q. J. R. Meteorol. Soc. 146, 1999–2049.
Hopcroft, P.O., Valdes, P.J., 2019. On the role of dust-climate feedbacks during the mid-holocene. Geophys. Res. Lett. 46, 1612–1621.
Huybers, P., 2006. Early pleistocene glacial cycles and the integrated summer insolation forcing. Science (1979) 313, 508–511.
Iskenderian, H., 1995. A 10-year climatology of northern hemisphere tropical cloud plumes and their composite flow patterns. J. Clim. 8, 1630–1637.
Jolly, D., Prentice, I.C., Bonnefille, R., Ballouche, A., Bengo, M., Brenac, P., Buchet, G., Burney, D., Cazet, J.-P., Cheddadi, R., Edorh, T., Elenga, H., Elmoutaki, S., Guiot, J., Laarif, F., Lamb, H., Lezine, A.-M., Maley, J., Mbenza, M., Peyron, O., Reille, M., Reynaud-Farrera, I., Riollet, G., Ritchie, J.C., Roche, E., Scott, L., Ssemmanda, I., Straka, H., Umer, M., Van Campo, E., Vilimumbalo, S., Vincens, A., Waller, M., 1998. Biome reconstruction from pollen and plant macrofossil data for Africa and the Arabian peninsula at 0 and 6000 years. J. Biogeogr. 25, 1007–1027.
Kaufman, D., McKay, N., Routson, C., Erb, M., Davis, B., Heiri, O., Jaccard, S., Tierney, J., Dätwyler, C., Axford, Y., Brussel, T., Cartapanis, O., Chase, B., Dawson, A., de Vernal, A., Engels, S., Jonkers, L., Marsicek, J., Moffa-Sánchez, P., Morrill, C., Orsi, A., Rehfeld, K., Saunders, K., Sommer, P.S., Thomas, E., Tonello, M., Tóth, M., Vachula, R., Andreev, A., Bertrand, S., Biskaborn, B., Bringué, M., Brooks, S., Caniupán, M., Chevalier, M., Cwynar, L., Emile-Geay, J., Fegyveresi, J., Feurdean, A., Finsinger, W., Fortin, M.-C., Foster, L., Fox, M., Gajewski, K., Grosjean, M., Hausmann, S., Heinrichs, M., Holmes, N., Ilyashuk, B., Ilyashuk, E., Juggins, S., Khider, D., Koinig, K., Langdon, P., Larocque-Tobler, I., Li, J., Lotter, A., Luoto, T., Mackay, A., Magyari, E., Malevich, S., Mark, B., Massaferro, J., Montade, V., Nazarova, L., Novenko, E., Pařil, P., Pearson, E., Peros, M., Pienitz, R., Płóciennik, M., Porinchu, D., Potito, A., Rees, A., Reinemann, S., Roberts, S., Rolland, N., Salonen, S., Self, A., Seppä, H., Shala, S., St-Jacques, J.-M., Stenni, B., Syrykh, L., Tarrats, P., Taylor, K., van den Bos, V., Velle, G., Wahl, E., Walker, I., Wilmshurst, J., Zhang, E., Zhilich, S., 2020. A global database of Holocene paleotemperature records. Sci. Data 7, 115.
Kim, S.T., Coplen, T.B., Horita, J., 2015. Normalization of stable isotope data for carbonate minerals: implementation of IUPAC guidelines. Geochim. Cosmochim. Acta 158, 276–289.
Kim, S.-T., O'Neil, J.R., 1997. Equilibrium and nonequilibrium oxygen isotope effects in synthetic carbonates. Geochim. Cosmochim. Acta 61, 3461–3475.
Kim, S.-T., O'Neil, J.R., Hillaire-Marcel, C., Mucci, A., 2007. Oxygen isotope fractionation between synthetic aragonite and water: influence of temperature and Mg2+ concentration. Geochim. Cosmochim. Acta 71, 4704–4715.
Knippertz, P., 2003. Tropical–Extratropical Interactions Causing Precipitation in Northwest Africa: statistical Analysis and Seasonal Variations. Mon. WEATHER Rev. 131, 8.
Knippertz, P., 2007. Tropical–extratropical interactions related to upper-level troughs at low latitudes. Dyn. Atmospheres Oceans 43, 36–62.
Knippertz, P., Fink, A.H., Reiner, A., Speth, P., 2003. Three Late Summer/Early Autumn Cases of Tropical–Extratropical Interactions Causing Precipitation in Northwest Africa. Mon. WEATHER Rev. 131, 20.
Kuhlmann, H., Meggers, H., Freudenthal, T., Wefer, G., 2004. The transition of the monsoonal and the N Atlantic climate system off NW Africa during the Holocene. Geophys. Res. Lett. 31, 1–4.
Kutzbach, J., Bonan, G., Foley, J., Harrison, S.P., 1996. Vegetation and soil feedbacks on the response of the African monsoon to orbital forcing in the early to middle Holocene. Nature 384, 623–626.
Kutzbach, J.E., Guan, J., He, F., Cohen, A.S., Orland, I.J., Chen, G., 2020. African climate response to orbital and glacial forcing in 140,000-y simulation with implications for early modern human environments. Proc. Natl. Acad. Sci. U. S. A. 117, 2255–2264.
Larrasoaña, J.C., Roberts, A.P., Rohling, E.J., 2013. Dynamics of Green Sahara periods and their role in hominin evolution. PLoS. One 8.
Lézine, A.M., Hély, C., Grenier, C., Braconnot, P., Krinner, G., 2011. Sahara and Sahel vulnerability to climate changes, lessons from Holocene hydrological data. Quat. Sci. Rev. 30, 3001–3012.
Maley, J., 1977. Palaeoclimates of Central Sahara during the early Holocene. Nature 269, 573–577.
Manning, K., Timpson, A., 2014. The demographic response to holocene climate change in the Sahara. Quat. Sci. Rev. 101, 28–35.
Marcott, S.A., Shakun, J.D., Clark, P.U., Mix, A.C., 2013. A reconstruction of regional and global temperature for the past 11,300 years. Science (1979) 339, 1198–1201.
McGee, D., deMenocal, P.B., Winckler, G., Stuut, J.B.W., Bradtmiller, L.I., 2013. The magnitude, timing and abruptness of changes in North African dust deposition over the last 20,000 yr. Earth Planet. Sci. Lett. 371–372, 163–176.
Mcguirk, J.P., Thompson, A.H., Smith, N.R., 1987. Moisture bursts over the tropical Pacific Ocean. Mon. Weather Rev. 115, 787–798.
Pausata, F.S.R., Gaetani, M., Messori, G., Berg, A., Maia de Souza, D., Sage, R.F., deMenocal, P.B., 2020. The Greening of the Sahara: past Changes and Future Implications. One Earth. 2, 235–250.
Pausata, F.S.R., Messori, G., Zhang, Q., 2016. Impacts of dust reduction on the northward expansion of the African monsoon during the Green Sahara period. Earth Planet. Sci. Lett. 434, 298–307.
Pausata, F.S.R., Zhang, Q., Muschitiello, F., Lu, Z., Chafik, L., Niedermeyer, E.M., Stager, J.C., Cobb, K.M., Liu, Z., 2017. Greening of the Sahara suppressed ENSO activity during the mid-Holocene. Nat. Commun. 8, 16020.
Perez-Sanz, A., Li, G., González-Sampériz, P., Harrison, S.P., 2014. Evaluation of modern and mid-Holocene seasonal precipitation of the Mediterranean and northern Africa in the CMIP5 simulations. Clim. Past 10, 551–568.
Phelps, L.N., Broennimann, O., Manning, K., Timpson, A., Jousse, H., Mariethoz, G., Fordham, D.A., Shanahan, T.M., Davis, B.A.S., Guisan, A., 2020. Reconstructing the climatic niche breadth of land use for animal production during the African Holocene. Glob. Ecol. Biogeogr. 29, 127–147.
Quade, J., Dente, E., Armon, M., Ben Dor, Y., Morin, E., Adam, O., Enzel, Y., 2018. Megalakes in the Sahara? A review. Quat. Res. 90, 253–275.
Raj, J., Bangalath, H.K., Stenchikov, G., 2019. West African Monsoon: current state and future projections in a high-resolution AGCM. Clim. Dyn. 52, 6441–6461.
Ramsey, C.B., 2009. Bayesian Analysis of Radiocarbon Dates. Radiocarbon. 51, 337–360.
Ramsey, C.B., Lee, S., 2013. Recent and planned developments of the program OxCal. Radiocarbon. 55, 720–730.
Repschläger, J., Garbe-Schönberg, D., Weinelt, M., Schneider, R., 2017. Holocene evolution of the North Atlantic subsurface transport. Clim. Past 13, 333–344.
Schneider, T., Bischoff, T., Haug, G.H., 2014. Migrations and dynamics of the intertropical convergence zone. Nature 513, 45–53.
Schwanghart, W., Scherler, D., 2014. Short Communication: topoToolbox 2 – MATLAB-based software for topographic analysis and modeling in Earth surface sciences. Earth Surf. Dyn. 2, 1–7.
Sha, L., Ait Brahim, Y., Wassenburg, J.A., Yin, J., Peros, M., Cruz, F.W., Cai, Y., Li, H., Du, W., Zhang, H., Edwards, R.L., Cheng, H., 2019. How Far North Did the African monsoon fringe expand during the African humid period? Insights from southwest Moroccan speleothems. Geophys. Res. Lett. 93–102.
Shi, X., Cauquoin, A., Lohmann, G., Jonkers, L., Wang, Q., Yang, H., Sun, Y., Werner, M., 2023. Simulated stable water isotopes during the mid-Holocene and pre-industrial periods using AWI-ESM-2.1-wiso. Geosci. Model Dev. 16, 5153–5178.
Skinner, C.B., Poulsen, C.J., 2016. The role of fall season tropical plumes in enhancing Saharan rainfall during the African Humid Period. Geophys. Res. Lett. 43, 349–358.
Thepenir, R.-M., Cruette, D., 1981. Formation of Cloud Bands Associated with the American subtropical jet stream and their interaction with midlatitude synoptic disturbances reaching Europe. Mon. Weather Rev. 109, 2209–2220.
Thompson, A.J., Tabor, C.R., Poulsen, C.J., Skinner, C.B., 2021. Water isotopic constraints on the enhancement of the mid-Holocene West African monsoon. Earth Planet. Sci. Lett. 554, 116677.
Tierney, J.E., Pausata, F.S.R., De Menocal, P.B., 2017. Rainfall regimes of the Green Sahara. Sci. Adv. 3, 1–10.
Tremaine, D.M., Froelich, P.N., Wang, Y., 2011. Speleothem calcite farmed in situ: modern calibration of δ18O and δ13C paleoclimate proxies in a continuously-monitored natural cave system. Geochim. Cosmochim. Acta 75, 4929–4950.
Trouet, V., Van Oldenborgh, G.J., 2013. KNMI Climate Explorer: a Web-Based Research Tool for High-Resolution Paleoclimatology. Tree-Ring Res 69, 3–13.
Vaks, A., Bar-Matthews, M., Matthews, A., Ayalon, A., Frumkin, A., 2010. Middle-late quaternary paleoclimate of northern margins of the Saharan-Arabian Desert: reconstruction from speleothems of Negev Desert, Israel. Quat. Sci. Rev. 29, 2647–2662.
Wassenburg, J.A., Dietrich, S., Fietzke, J., Fohlmeister, J., Jochum, K.P., Scholz, D., Richter, D.K., Sabaoui, A., Spötl, C., Lohmann, G., Andreae, M.O., Immenhauser, A., 2016. Reorganization of the North Atlantic oscillation during early Holocene deglaciation. Nat. Geosci. 9, 602–605.
Ziv, B., 2001. A subtropical rainstorm associated with a tropical plume over Africa and the Middle-East. Theor. Appl. Climatol. 69, 91–102.